International Journal of Bioprinting

RESEARCH ARTICLE

Designing an anatomical contour titanium 3D-printed oblique lumbar interbody fusion cage with porous structure and embedded fixation screws for patients with osteoporosis

Po-Liang Lai[1], Shao-Fu Huang[2], Hsuan-Wen Wang[2], Pei-Hsin Liu[2], Chun-Li Lin[3]*

[1]Department of Orthopedic Surgery, Bone and Joint Research Center, Chang Gung Memorial Hospital at Linkou, College of Medicine, Chang Gung University, Taoyuan City, Taiwan

[2]Department of Biomedical Engineering, National Yang Ming Chiao Tung University, Hsinchu, Taiwan

[3]Department of Biomedical Engineering, Medical Device Innovation & Translation Center, National Yang Ming Chaio Tung University, Hsinchu, Taiwan

Abstract

This study aimed to design an anatomical contour metal three-dimensional (3D)-printed oblique lateral lumbar interbody fusion (OLIF) cage with porous (lattices) structure and embedded screw fixation to enhance bone ingrowth to reduce the risk of cage subsidence and avoid the stress-shielding effect. Finite element (FE) analysis and weight topology optimization (WTO) were used to optimize the structural design of the OLIF cage based on the anatomical contour morphology of patients with osteoporosis. Two oblique embedded fixation screws and lattice design with 65% porosity and average pore size of 750 μm were equipped with the cage structure. The cage was fabricated via metal 3D printing, and static/dynamic compression and compressive-shear tests were performed in accordance with the ASTM F2077-14 standard to evaluate its mechanical resistance. On FE analysis, the OLIF cage with embedded screw model had the most stability, lowest stress values on the endplate, and uniform stress distribution versus standalone cage and fixed with lateral plate under extension, lateral flexion, and rotation. The fatigue test showed that the stiffnesses/endurance limits (pass 5 million dynamic test) were 16,658 N/mm/6000 N for axial load and 19,643 N/mm/2700 N for compression shear. In conclusion, an OLIF cage with embedded fixation screws can be designed by integrating FE and WTO analysis based on the statistical results of endplate morphology. This improves the stability of the OLIF cage to decrease endplate destruction. The complex contour and lattice design of the OLIF cage need to be manufactured via metal 3D printing; the dynamic axial compression and compressive-shear strengths are greater than that of the U.S. Food and Drug Administration (FDA) standard.

Keywords: Oblique lumbar interbody fusion; Cage; 3D printing; Finite element; Topological optimization

***Corresponding author:**
Chun-Li Lin
(cllin2@nycu.edu.tw)

Citation: Lai P-L, Huang S-F, Wang H-W, *et al*., 2023, Designing an anatomical contour titanium 3D-printed oblique lumbar interbody fusion cage with porous structure and embedded fixation screws for patients with osteoporosis. *Int J Bioprint*, 9(5): 772. https://doi.org/10.18063/ijb.772

Received: January 27, 2023
Accepted: April 6, 2023
Published Online: June 13, 2023

1. Introduction

Lumbar interbody fusion is an effective and common treatment of spine-related diseases. Alongside the development of minimally invasive surgery, the technique of oblique lateral lumbar interbody fusion (OLIF) has also recently been developed, which reduces the risk of wound infection, minimizes muscle/soft tissue cutting, and involves a shorter operation time[1,2]. During surgery, a larger-area cage can be expected to provide greater spinal stability, but the resulting vertebral instability can lead to cage subsidence[1,2]. In particular, patients with osteoporosis have unstable spines and are at a higher risk of cage subsidence when managed with an OLIF cage alone[2,3].

Combining the posterior pedicle screw fixations with the OLIF cage can reduce surgical complications and prevent cage subsidence[2,3]. However, the use of pedicle screws increases surgical burden and causes additional wounds when being implanted into the spine bodies. One approach to enhance OLIF cage stability is through additional anterior fixation with a lateral bone plate. Nevertheless, protrusion of the lateral bone plate was prone to surrounding tissue wear and damage as the clinical complication[4,5]. Therefore, embedding screws within the OLIF cage can directly fix the cage and the vertebral body through surgical insertion.

Some studies have pointed out that the contact area between the cage and the endplate can affect subsidence[6], and the contour of the superior/inferior surface of the cage was related to the morphology of the endplate. The point contact at the surface of the endplate easily causes stress concentration and endplate damage, resulting in a higher risk of subsidence. In recent years, an anatomical titanium alloy cage that conforms to the physiological appearance of a patient-specific endplate was proposed to reduce stress concentration[7]. However, the clinical application of anatomical titanium alloy cage is limited because of its complicated design and time-consuming manufacturing processes.

Nevertheless, a structure that assists bone ingrowth is needed to achieve effective bone fusion between the cage and the endplate[8]. Replacing the surface of the cage with a porous (lattice) biomimetic microstructure can effectively promote the differentiation and growth of osteocytes attached to the pore structure[9,10]. It is well known that pore design with 60%–70% porosity and pore size under 800 μm, manufactured using AM, provide biologically active and mechanically stable surfaces for implant fixation to bone[10-12]. However, a complex structure with a high-precision hybrid design of the cage cannot be fabricated by the traditional mechanical cutting process, and thus, there is a need to employ metal three-dimensional (3D) printing, which can create a porous structure on a dense titanium body[9-15].

The objective of this study was to design an anatomical contour OLIF cage based on the anatomical surface morphology of patients with osteoporosis. We aim to design an optimal structure with lattices structure to enhance bone ingrowth and embedded screw fixation to increase the stability. This OLIF cage was fabricated via metal 3D printing and tested using the fatigue biomechanical test to confirm whether its characteristic is in compliance with the criteria set by U.S. Food and Drug Administration (FDA).

2. Materials and methods

2.1. Finite element model generation and validation

A previously validated finite element (FE) model was used in our mechanical simulation analysis, and a brief description of the generation method is given below[16]. A 70-year-old female without severe bone spurs, fractures, and scoliosis was selected as a volunteer, and computed tomography (CT) scans were performed using a 0.625-mm interval to reconstruct lumbar vertebrae mock-ups of the L2–L5 lumbar vertebrae. The solid model includes cortical bone, cancellous bone, endplates, intervertebral discs (nucleus and annulus fibrosus), and facet joints (with a 1-mm gap). The ligaments associated with L2 to L5 were constructed according to their anatomical location (Figure 1)[17].

The lumbar spine solid model was exported to the ANSYS Workbench (ANSYS Workbench v18.2, ANSYS Inc., PA, USA) for simulation. Mesh generation was performed using quadratic ten-node tetrahedral structural solid elements, and the mesh model accommodated a total of 689,810 elements and 1,022,598 nodes (Figure 1)[16]. The material properties of cortex, cancellous bone, endplates, and intervertebral discs were linear elastic and isotropic and were adopted from the literature (Table 1)[14,18]. All ligaments used the hyperelastic Ogden third-order formula for material properties[14,18]. The facet joint used a contact element with a friction coefficient of 0.2 to simulate the sliding mechanism of the joint surfaces. It was validated that this FE model is reliable when it reaches a reduced order model (ROM) for L3–L4 variation within 20% of that reported by Yamamoto *et al.*[19-21].

2.2. OLIF cage design

To simulate the morphology of vertebral endplates with osteoporosis in elderly patients, the average morphological subsidence of L2–L5 endplates in 20 elderly patients with osteoporosis was obtained[16,22]. Endplate subsidence was calculated at 25%, 50%, and 75% of the endplate length in both the coronal and sagittal planes (Figure 1), and the FE model was modified to represent the endplate concave characteristics.

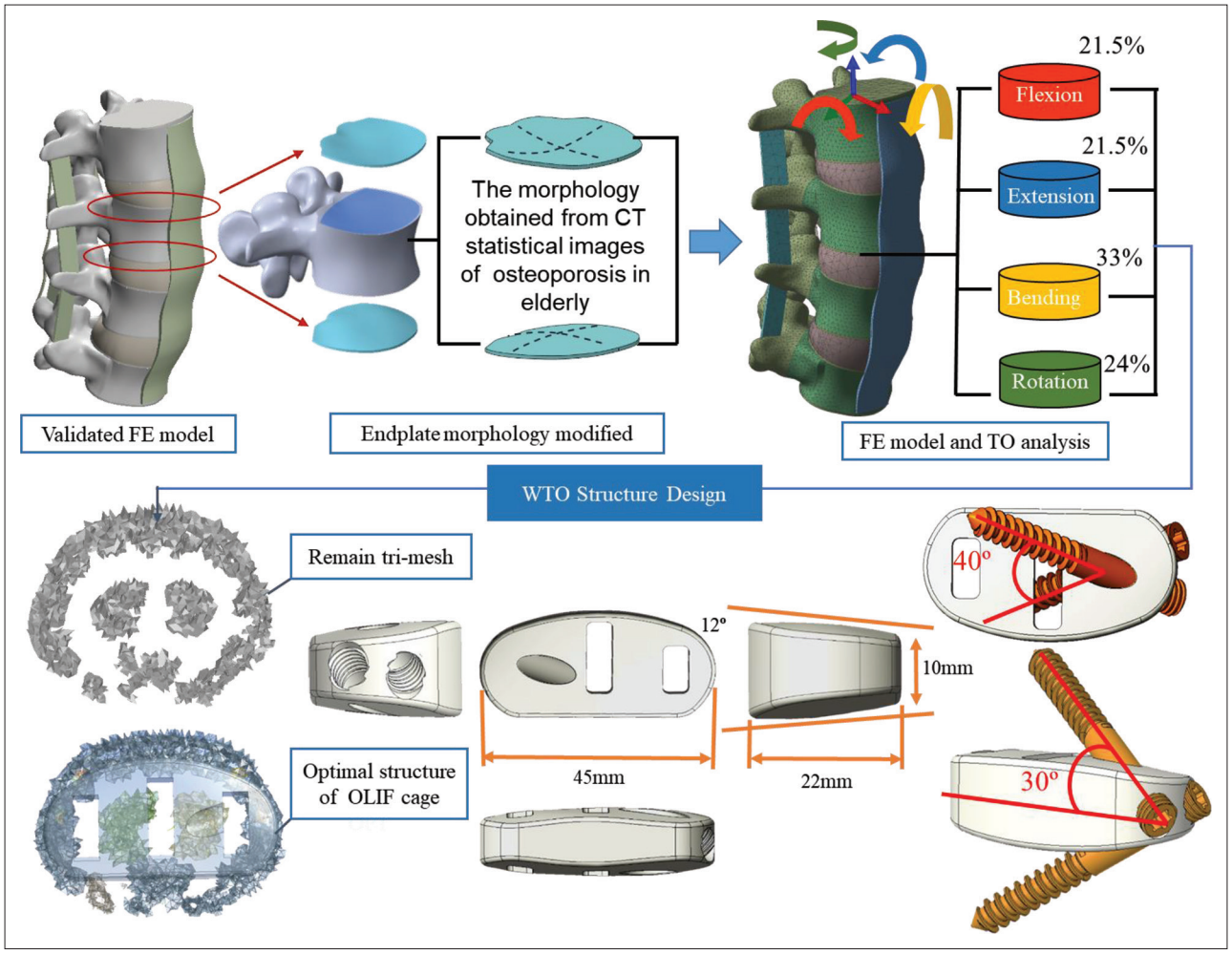

Figure 1. Design process of the oblique lateral lumbar interbody fusion (OLIF) cage included FE model based on the endplate morphology obtained from osteoporosis in elderly and WTO. Right bottom part shows the detail dimensions of the OLIF cage.

Table 1. Material property simulated during finite element analysis

Material	Young modulus (MPa)	Poisson's ratio
Cortex bone	12,000	0.3
Cancellous bone	100	0.2
Endplate	4000	0.25
Core	1	0.499
Annulus fiber	4.2	0.45
OLIF cage (Ti6Al4V)	110,000	0.3
Bone plate (Ti6Al4V)	110,000	0.3
Screw (Ti6Al4V)	110,000	0.3

Using the topology optimization (TO) analysis provided in ANSYS Workbench, the L3–L4 intervertebral disc region was designed to optimize individually the structure with sufficient strength under flexion, extension, bending, and axial rotation of the spine (applied axial loads of 150 N on the upper endplate of L2, as well as separate load conditions of 10 N-m, 7.5 N-m, 10 N-m, and 10 N-m for flexion, extension, bending, and axial rotation, respectively). Since the lumbar spine was subjected to 21.5% flexion and extension, 33% lateral bending, and 24% axial rotation to represent various load ratios during daily activities[23,24], the final intervertebral disc structure was obtained by multiplying four respective weight coefficients of different loads through the weight topology optimization (WTO) (Figure 1)[16].

The outline of the OLIF cage was simplified based on the triangular mesh regions recommended by the WTO results to ensure that the cage maintains sufficient strength under physiological loads. Specifically, this was simplified to a 45 × 22 mm ellipse, 10 mm height, and 12° anterior and posterior tilt. The contour features of the superior/inferior cage surfaces were based on the morphology

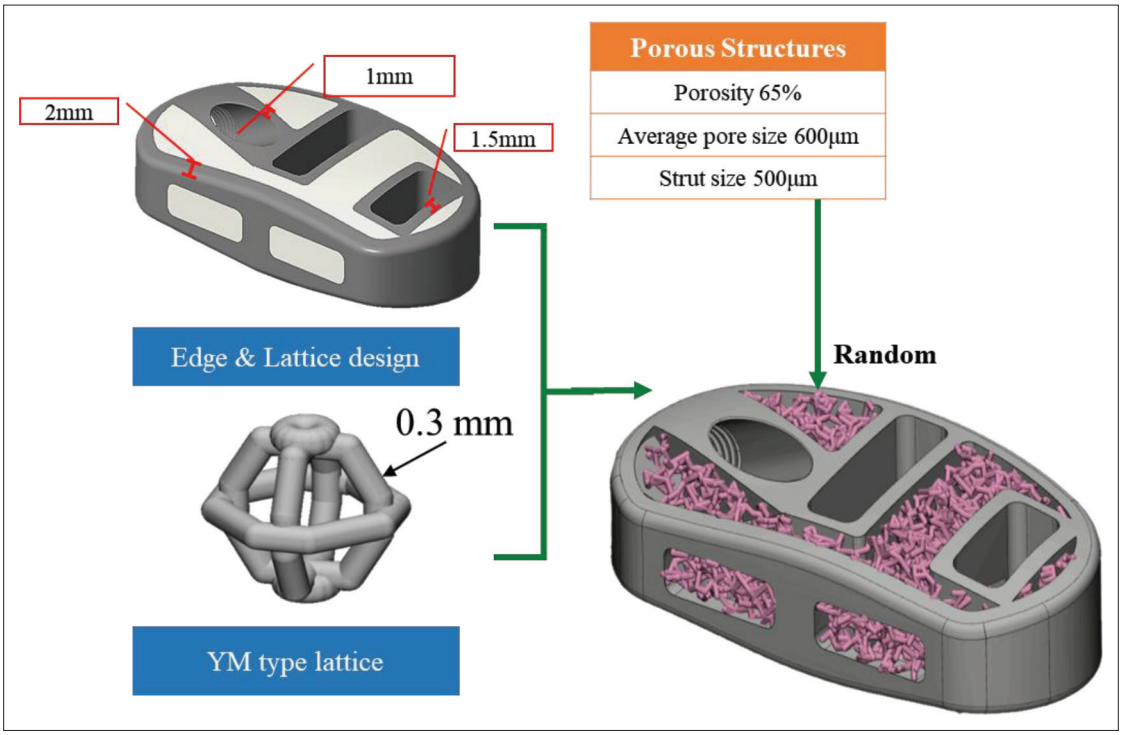

Figure 2. The YM lattice was designed with a spherical structure (pillar diameter of Ø 0.3 mm) and arranged in the hollow part of the oblique lateral lumbar interbody fusion (OLIF) cage. The porosity of each lattice was set to 65%, and the pore size was set at 600–900 μm.

counted by previous osteoporosis patients. Two threaded oblique holes were established on the superior and inferior surfaces of the cage to facilitate the insertion of fixation screws. To obtain the best screw fixation strength and avoid screw loosening, two screws were placed 30° up and down the transverse plane and staggered at 40° angles anteriorly and posteriorly (Figure 1).

To reduce the stress-shielding effect caused by the high elastic modulus and increase the bone fusion efficiency of the OLIF cage, the peripheral region wall thickness, bone fusion groove contours, and that around the screw hole of the cage were set 2, 1.5, and 1 mm, respectively. The bone fusion groove was filled and randomly arranged in a $SU(N_c)$ Yang-Ming (YM) lattice, which was designed as a multi-corner spherical structure for excepting cell clustering with a 1-mm^3 unit cube and a pillar diameter of Ø 0.3 mm. The porosity of each lattice was set to 65%, and pore size was controlled at a range of 600–900 μm according to literatures' suggestion (Figure 2)[11,12,25].

2.3. Finite element analysis

Three simulated models included depending on where the OLIF cage was implanted: (i) along the L3–L4 disc (noted as CA), (ii) in the L3-L4 disc with two screws embedded in L3 and L4 (5.5 mm in diameter and 40 mm in length; noted as CES), and (iii) in the L3–L4 disc and two lateral screws (5.5 mm in diameter and 40 mm in length) placed in the L3 and L4 bodies with a lateral fixation plate (noted as CLS). All three models underwent FE simulations to understand the mechanical responses between different implant combinations (Figure 3).

Three models of CA, CES, and CLS were meshed using quadratic ten-node tetrahedral structural solid elements, with their corresponding eminent/node numbers of 464762/723280, 442500/740485, and 513566/809520, respectively. The Ti6Al4V was assigned as the material property for the cage, screw, and lateral fixation plate. Other material properties and loading and boundary conditions were the same with previous section of FE model generation and validation.

The ROM between L3 and L4 and stress distribution at the superior endplate of the L4 was recorded to evaluate the stability of different fixation systems. ROM was defined as the variation of the rotation angle of the adjacent lumbar vertebral bodies. The rotation angle of a single vertebral body was obtained by calculating the dot production of a fixed vector, which was formed by the same two feature points within the vertebral body, before and after simulations.

2.4. OLIF cage 3D printing and functional fatigue test

The OLIF cage randomly filled with YM lattice in the bone fusion grooves was fabricated using a metal 3D printer

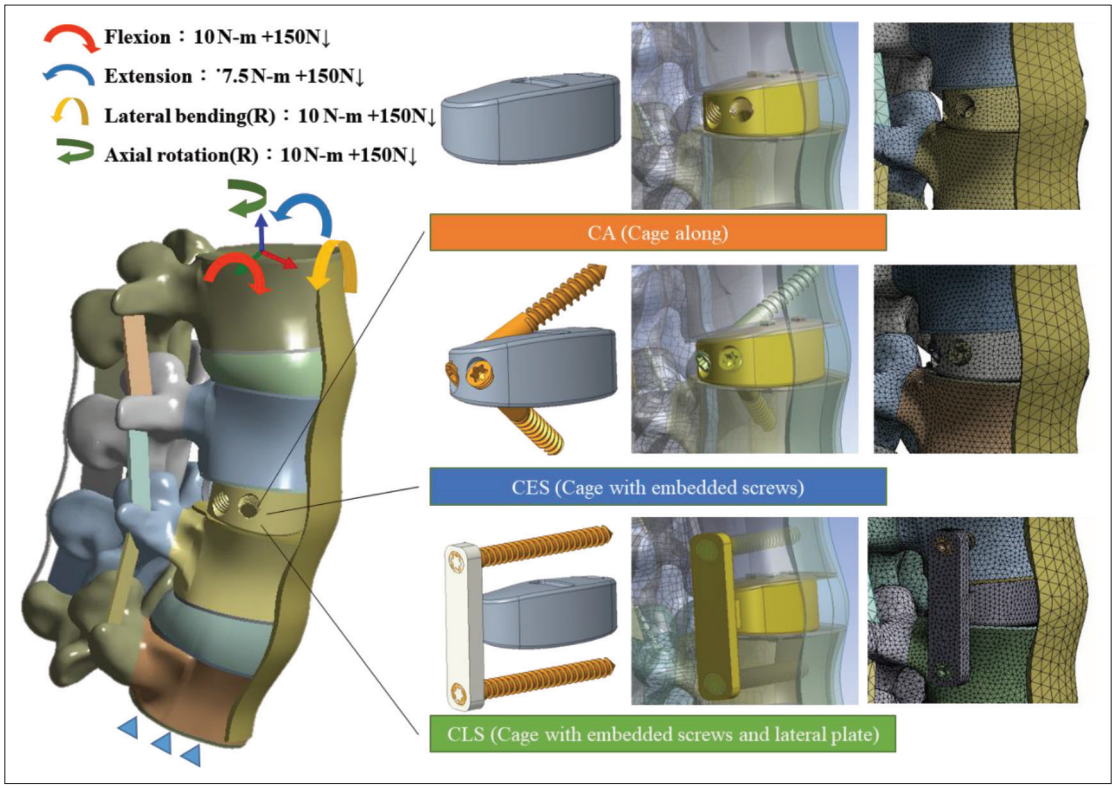

Figure 3. Three simulated models included depending on where the oblique lateral lumbar interbody fusion (OLIF) cage was implanted: (1) along the L3–L4 disc (CA, right upper part), (2) in the L3-L4 disc with 2 screws embedded in L3 and L4 (5.5 mm in diameter and 40 mm in length; CES, right middle part), and (3) in the L3–L4 disc and 2 lateral screws (5.5 mm in diameter and 40 mm in length) placed in the L3 and L4 bodies with a lateral fixation plate (CLS, right bottom part).

(AM250, Renishaw, Gloucestershire, UK) using titanium alloy powder (Ti6Al4V ELI powder ranges between 15 μm and 45 μm in diameter). This OLIF cage was stored at 23°C room temperature and 30%–60% relative humidity (Figure 4)[22]. The 3D printing machine was operated with a laser power of 200 W, a scanning rate of 0.6 m/s, and an exposure time of 125 s. The powder was selectively scanned and melted by a laser during the process. The fabricated component could be made after the powder was crystallized. The manufacturing accuracy and layer thickness in this study were both 30 μm, respectively. Completed cages were removed for deburring and polishing using a magnetic polisher with stainless steel pins (Ø = 1 mm, L = 3 mm) at 2700 rpm speed and cleaned using ultrasonic oscillations (Figure 4)[24]. Our 3D printer laboratory was approved by the ISO13485 quality management system (Certificate Number: 1760.190828) to ensure that the implants meet the necessary regulations, thus assuring safety and quality. After 3D printing, the OLIF cage was acid-etched to remove residual sandblast particles and cleaned using ultrasonic oscillations (Figure 4)[24].

For analysis on the dimensional accuracy and surface roughness of the 3D-printed cage, the detailed dimensions of all OLIF cage features in the computer-aided design (CAD) software were defined as the actual dimensions. The 3D-printed manufacturing dimensions, length (L), height (H1, H2, H3), width (W), slot length (SL1, SL2), and slot width (SW1, SW2) (see Figure 5) were measured using a precision measuring system (ARCS Precision Technology Co., Ltd., Taiwan) on three randomly selected OLIF cages and compared with the corresponding actual values. Surface roughness (Ra) on the three pieces (PW1, PW2, and PW3) with 4-mm length at the posterior side of three randomly selected OLIF cages was measured using a portable measuring instrument with 0.006 μm resolution (SJ-210, Mitutoyo Co, Ltd., Tokyo, Japan) (Figure 5).

Static/dynamic compression and compressive-shear tests in accordance with the ASTM F2077-14 standard were performed to evaluate the mechanical resistance of the OLIF cage and to assess compliance with FDA-recommended values[26]. The superior and inferior parts of each of three 3D printing OLIF cages were clamped using specific jigs on the material test machine according to the ASTM2077 for the different test groups (Figures 6a and 7a).

Figure 4. The oblique lateral lumbar interbody fusion (OLIF) cage fabricated by a metal 3D printer; (a) without fixation screws and (b) with embedded fixation screws.

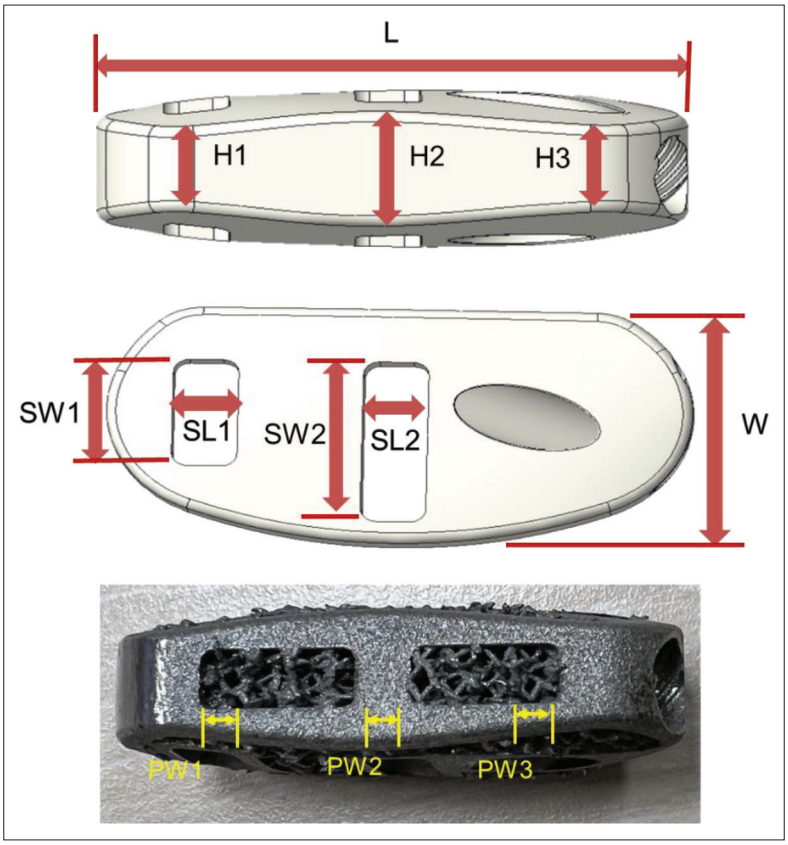

Figure 5. Measured point and position of 3D-printed cage dimensional accuracy and surface roughness.

For the static compression/compressive-shear tests, a 500 N preload was applied and a crosshead speed of 6 mm/min was applied until either the OLIF cage cracked/fractured, the force decreased below 20% of the maximum load, or until the testing machine limitation (UH-F500 KNI for compression test and Instron 8874 for compressive-shear test) (UH-F500 KNI, Shimadzu Corp., Kyoto, Japan and Instron, 8874, INSTRON, Canton, MA, USA) (Figures 6a and 7a). The load–displacement curves were recorded. The dynamic tests were then carried out according to the maximum load of the static compression/shear test. The maximum cyclic loads were set at 24,000 N (16%), 16,000 N (10.7%), 8000 N (5.33%), and 6000 N (4%) for the maximum compression load and 12,000 N (50%), 6000 N (25%), 3500 N (14.58%), and 2600 N (10.8%) for the shear load. The maximum difference between the load levels used for the dynamic loads determination shall be no greater than 10 % of the static maximum load or the testing machine limitation. The R value (Fm_{ax}/F_{min}) was set as 10 under a test frequency of 10 Hz. The OLIF cage endurance limit was set when the test passed 5,000,000 cyclic loads, and fracture/creak pattern of any component was observed. The observed OLIF cage crack on the surface was recorded by a non-contact precision measuring system (ARCS Precision Technology Co., Ltd., Taiwan) with magnification by 40 times.

3. Results

Figure 4 illustrates the OLIF cages with bone growth lattice with embedded fixation screws manufactured via 3D printing. We defined that the error for each dimension should be within 5%, namely, the printed accuracy of our OLIF cage should meet implant manufacture requirements. All manufacturing errors were found within 5% (maximum error of 3.40%), which showed that the metal 3D printing equipment used in this study has good precision and was suitable for medical applications (Table 2). The surface roughness mean (standard deviation) for PW1, PW2, and PW3 were 8.93 (0.38) μm, 8.98 (0.74) μm, and 9.52 (0.76) μm, respectively.

Figure 8 shows the FE results of L3–L4 ROM under four load conditions; these were substantially reduced in all implantation methods (CA, CES, and CLS models) compared to the intact model. The CA model demonstrated the largest ROM in all load cases across the three implantation methods. The CES model had the most stability under extension, lateral flexion, and rotation. The

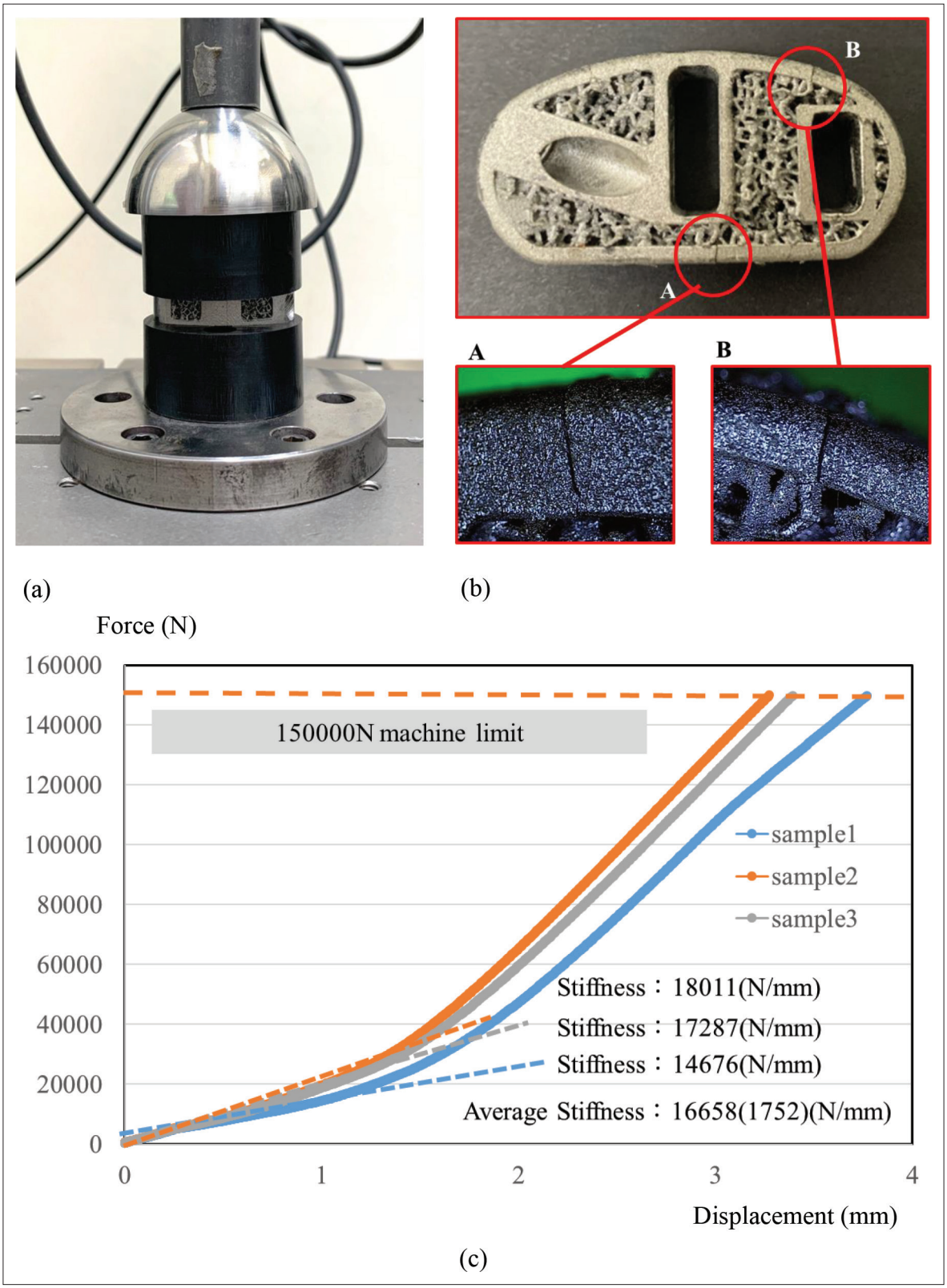

Figure 6. (a) Experimental setup illustration of the static/fatigue compression test for the oblique lateral lumbar interbody fusion (OLIF) age; (b) microcrack of the cage after fatigue test; and (c) stiffnesses of the static compression test.

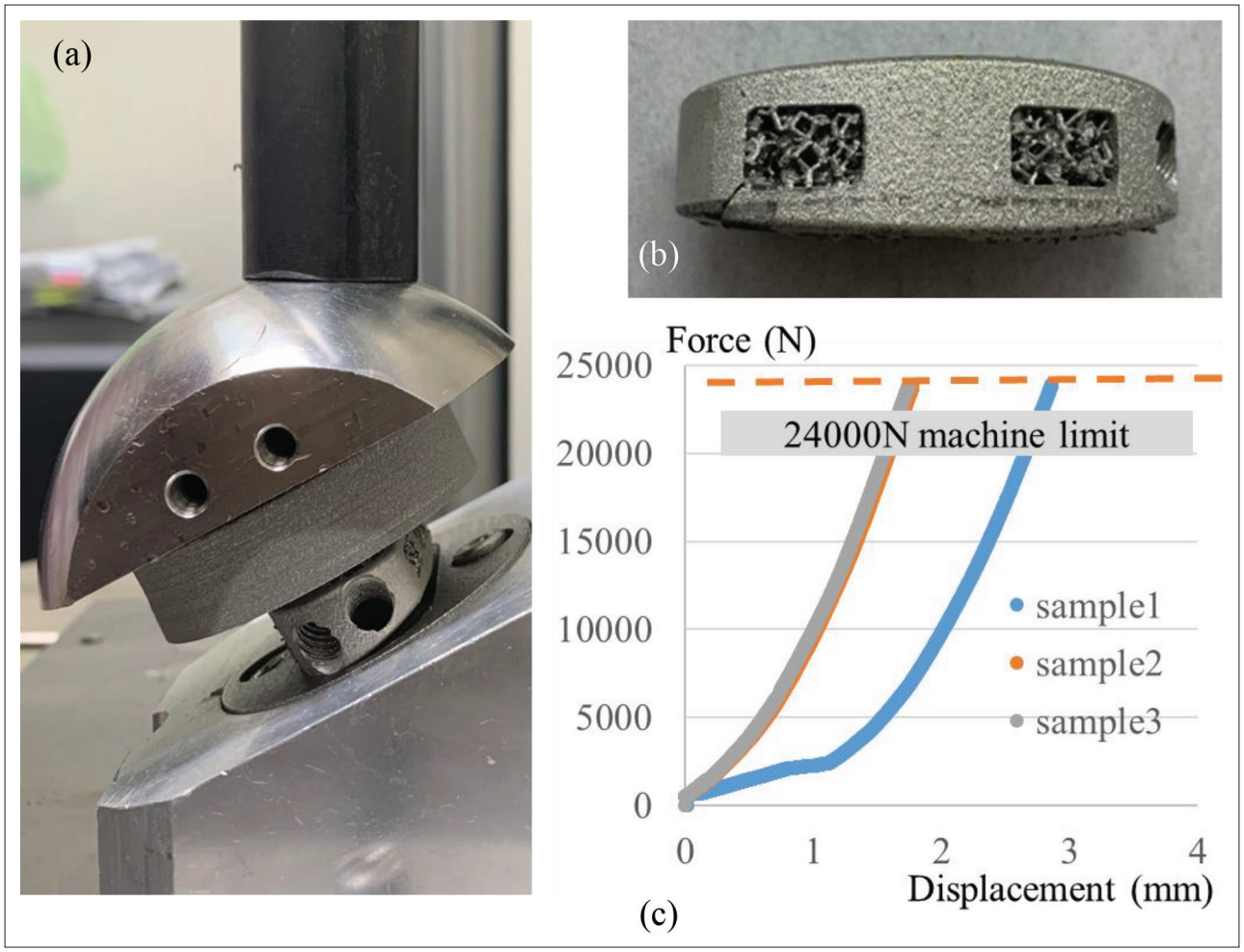

Figure 7. (a) Experimental setup illustration of the static/fatigue compression-shear test for the oblique lateral lumbar interbody fusion (OLIF) age; (b) microcrack of the cage after fatigue test; and (c) stiffnesses of the static compression-shear test.

CLS model exhibited the best performance in flexion, with slightly poor ROMs under extension, lateral bending, and rotation than the CA model.

Figure 9 shows the distribution of von Mises stress on the endplate for the three models and their corresponding stress concentration locations under four load conditions. Across the three models, the highest stress values were found in flexion. The maximum von Mises stresses of the CES model under flexion, extension, lateral bending, and rotation were 43.94, 13.94, 12.75, and 15.82 MPa, respectively; these values were the lowest compared to the CA and CLS models. The locations of stress concentration were usually found at anterior/posterior edge around the OLIF cage, especially for CA and CLS implantations under extension and rotation.

The static compression tests were all up to 150,000 N (the maximum load), and tests were stopped once they reached this upper limit. None of the tested cages were deformed, damaged, or cracked. The average stiffness and standard deviation of static compression was 16,658 ± 1752 N/mm from the load–displacement curve (Figure 6c). Global rupture was observed for all cages at 860,000 and 1.22 million cyclic loads under 24,000 N (16% of the maximum load) and 16,000 N (10.7% of the maximum load), respectively. However, the endurance limits were found at 8000 N and 6000 N; global rupture was not observed when cyclic load passed 5 million, but microcracks were found at the anterior/posterior edge (Figure 6b).

The static compressive-shear test was set to stop upon reaching the upper limit of the testing machine at 24,000 N (the maximum load). None of the tested cages were deformed, damaged, or cracked. The load–displacement curve is shown in Figure 7. The average stiffness of the static compression-shear was obtained at 19,643 N/mm from load–displacement curve (Figure 7c). The dynamic compressive-shear test found that the global cage ruptured

Table 2. Result of 3D-printed cage dimensional accuracy

Dimension	Symbol			Actual dimension (mm)			3D-printed dimension Mean (error percentage %) (mm)		
Cage length	L			45.00			45.37 (0.82)		
Cage width	W			22.00			21.77 (-1.05)		
Cage height	H1	H2	H3	7.86	10.26	7.93	7.71 (-1.87)	10.34 (0.75)	7.84 (-1.18)
Slot width	SW1	SW2		10.00	15.00		10.19 (1.90)	15.14 (0.93)	
Slot length	SL1	SL2		5.00	5.00		5.17 (3.40)	4.89 (-2.27)	

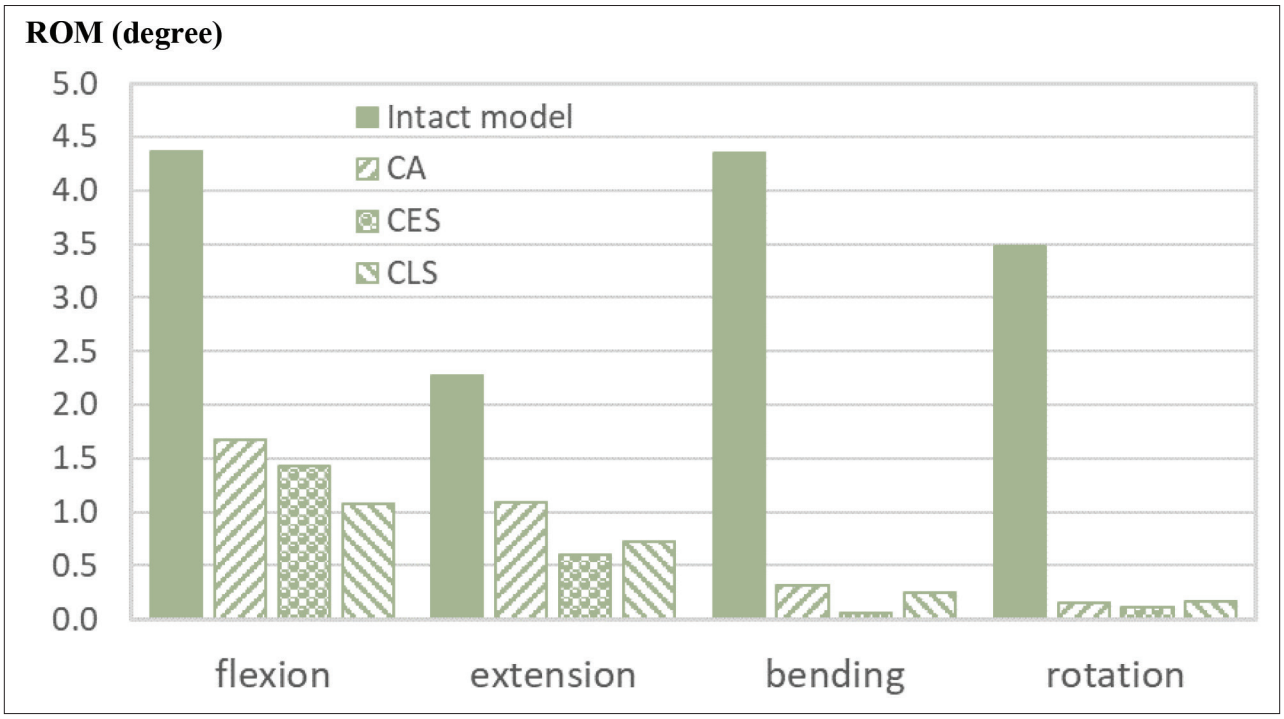

Figure 8. Range of motion for CA, CES, and CLS models under flexion, extension, bending, and torsion.

in the 12,000 N (50% of the maximum load) and 6000 N (25% of the maximum load) groups at 470,000 and 2.73 million cyclic loads, respectively. Cyclic tests could pass 5 million cycles under 3500 N, but microcracks occurred at the bottom edge of the cage. Therefore, the endurance limit was 2600 N for the compressive-shear test (Figure 7b and c).

4. Discussion

The OLIF approach can not only reduce the number of wounds but also cover a larger area compared to the traditional posterior lumbar interbody fusion approach. However, the superior/inferior surfaces of the current commercial OLIF cages are all flat and do not consider the morphological changes of the endplate in patients with osteoporosis. In addition, the stability of the commercial flat OLIF needs to be increased via lateral plate or posterior pedicel screw fixation, but this would increase the rate of clinical complications. Therefore, a better OLIF cage should consider the morphology of the superior/inferior surface to increase the contact surface to achieve good stress transfer, optimize the structure to reduce stress shielding, and improve the bionic lattice design to enhance the bone ingrowth effect.

In this study, the optimal disc region structure was obtained through feedback from the FE and WTO analysis under different activities with load on the disc simulating daily life. An OLIF cage profile was designed according to the optimized results based on the statistical results of endplate morphology from osteoporosis patients. Then, anterior/posterior cross and transverse plane tilted embedded locking fixation screws were combined with

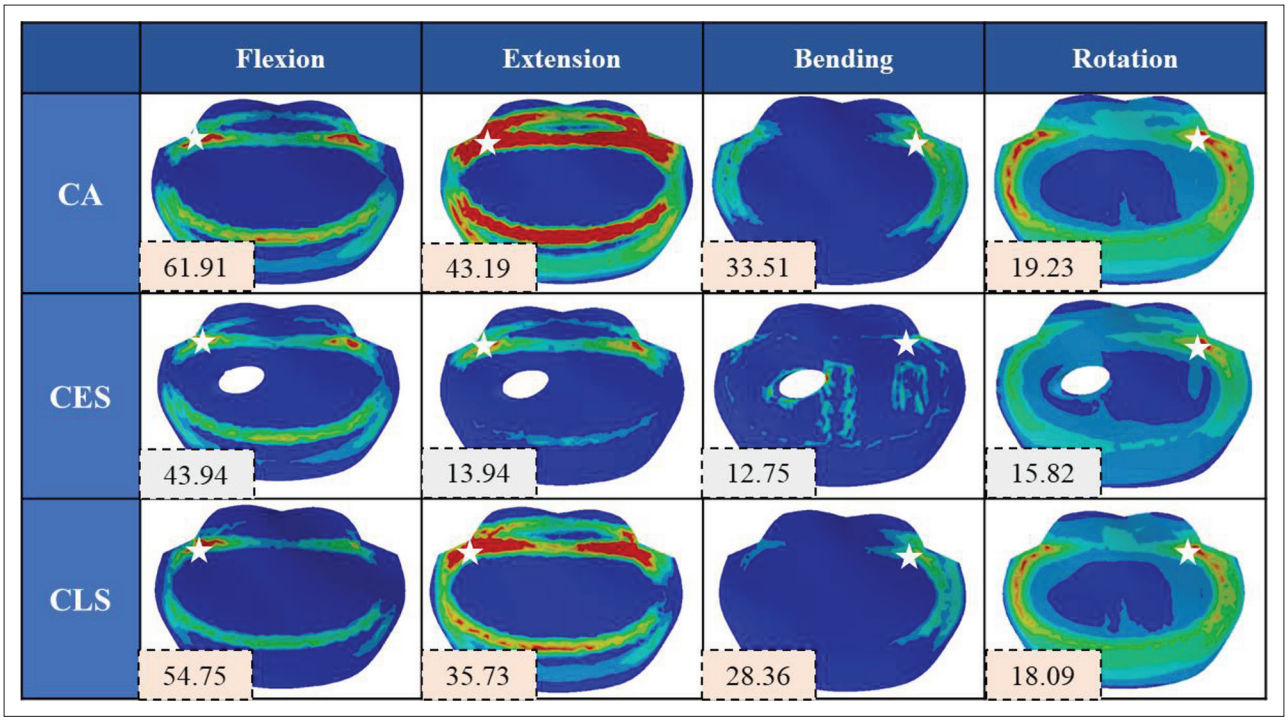

Figure 9. von Mises stress distributions for the intact, CA, CES, and CLS models under flexion, extension, bending, and torsion.

this cage profile to improve overall system stability after surgery[24].

Metal 3D printing techniques are well-established for building complicated 3D medical implants and have great potential to solve the problems of creating a porous titanium body[11,12,24]. Many studies have indicated that titanium implants manufactured via 3D printing with a porous design can enhance bone stability through enough bone ingrowth[11,12,24]. Therefore, the hollow part within the cage and exterior walls of the cage without the supporting solid structure was designed as grooves according to the suggestion of the WTO analysis. This was filled with YM lattice, which has good performance in terms of bone ingrowth capability and bonded strength between the implant and bone. This reduces the stress-shielding effect while increasing bone growth and improving overall stability.

Lumbar interbody fusion surgery aims to increase the stability (i.e., decrease the ROM) between two vertebral bodies is the main goal. The results of FE analysis showed that CA implantation reduced the ROM by 62%, 52%, 93%, and 96% under flexion, extension, lateral bending, and rotation, respectively, compared to the intact model. ROM decreased by an average of about 75%. The relative decreased percentages of the CES and CLS implantations under the aforementioned four load conditions were 67%/73%/99%/97% and 75%/68%/94%/95%, respectively, with a relative overall decrease of approximately 84% and 83% in ROM, respectively. The CES model demonstrated better stability among all implantations regardless of load condition. However, the decrease in ROM of the three fixation methods in terms of bending and rotation was greater than that of flexion and extension, consistent with a previous study[15]. Furthermore, the CES model was also comparable to the lateral enhanced fixation of CLS, which can provide higher stability especially in flexion.

Excessive stress on the endplate may result in destruction or fracture of the endplate. Thus, it is necessary to confirm whether the vertebral cage system induces unfavorable stress on the endplate during implantation. On FE analysis, we found that contact areas at the anterior/posterior edges between the cage and endplate during CES implantation can effectively reduce stress values and distribution to decrease endplate damage and the risk of cage subsidence especially during extension. This suggests that our OLIF cage with the embedded fixation screws can more effectively transmit cage force to the endplate than that with lateral plate fixation. This result was in line with the previous ROM results.

Complex contours and the internal lattice design of the OLIF cage only can be fabricated by 3D printing rather than traditional mechanical cutting. Previous

studies report that 3D printing techniques have great potential to solve the problems of creating a porous (lattice) surface coating on dense titanium and a porous titanium body[10-12,27,28]. Therefore, this study utilized metal 3D printing to manufacture our OLIF cage to perform functional tests. Our 3D printer laboratory was approved by the ISO13485 quality management system (Certificate Number: 1760.190828) to ensure that the implants meet the necessary regulations and to ensure safety and quality.

The stiffness measured under axial load was 16,658 N/mm, and the endurance limit after 5 million dynamic tests was 6000 N[26,29,30]. These values were more than double the minimum battery of performance testing necessary for stiffness at 7690 N/mm and endurance limit at 3000 N as recommended by the FDA. However, it was prone to cracks at edge of the cage under 6000 N of cyclic force, suggesting that the cage had insufficient support strength at the edge. It may be necessary to increase the edge wall thickness of the cage to enhance strength and maintain tissue permeability and bone growth range. Post-processing can also be considered to improve the lack of toughness in metal 3D printing.

The OLIF cage was not deformed, damaged, or cracked when the testing force reached the upper limit of the machine capability of 24,000 N during the static compressive-shear test. Therefore, this value (24,000 N) was denoted as the ultimate compressive-shear strength. This was higher than 95% of the vertebral cage strength values reported in the literature[26,29,30]. The corresponding stiffness can also be obtained as 19,643 N/mm, which is more than 8.85 times the FDA-recommended value of 2219 N/mm. For the shear fatigue test, the OLIF cage was prone to damage on the anterior edge during the dynamic high-strength fatigue compression-shear test above 3500 N. This phenomenon was consistent with the results of the aforementioned dynamic axial compressive test, implying that the cage edge thickness may need to be improved. The endurance limit was at 2600 N for the compressive-shear dynamic test, which is double the FDA-recommended limit of 1225 N[26].

The embedded screws were not considered during the compression/compressive-shear tests, which were conducted in accordance with the ASTM 2077 regulations recommended by the FDA[26]. The results of this test are comparable to the recommended minimum battery performance of the benchmark under the same testing conditions. Nevertheless, it may be necessary to perform *in vivo* animal experiments in the future to evaluate the fixation ability of embedded bone screws and the bone growth ability within cage lattices.

5. Conclusion

A new OLIF cage with embedded fixation screws was designed by integrating the FE and WTO analysis based on statistical results of endplate morphology. The simulated results showed that the embedded screw fixation can improve the stability of the OLIF cage and decrease endplate damage. The OLIF cage with lattice manufactured via metal 3D printing was subject to mechanical testing, and we found that the dynamic axial compression and compressive-shear tests exceeded FDA-recommended values by about two times. However, the edge design of the OLIF cage must undergo further improvements to increase resistance against dynamic strength.

Acknowledgments

Authors would like to thank Microware Precision Co., Ltd, Taiwan for their assistance in cage and screw manufacture.

Funding

This study is supported in part by MOST project 109-2622-B-010-005 and 110-2221-E-075-004, Taiwan.

Conflict of interest

The authors declare no conflicts of interest.

Author contributions

Conceptualization: Po-Liang Lai, Chun-Li Lin
Investigation: Shao-Fu Huang, Hsuan-Wen Wang, Pei-Hsin Liu
Methodology: Shao-Fu Huang, Hsuan-Wen Wang, Pei-Hsin Liu
Resources: Po-Liang Lai, Chun-Li Lin
Writing – original draft: Po-Liang Lai
Writing – review & editing: Chun-Li Lin

Ethics approval and consent to participate

Not applicable.

Consent for publication

Not applicable.

Availability of data

Not applicable.

References

1. Orita S, Inage K, Furuya T, *et al.*, 2017, Oblique lateral interbody fusion (OLIF): Indications and techniques. *Oper Tech Orthop*, 27(4): 223–230.

2. Zeng ZY, Xu ZW, He DW, *et al.*, 2018, Complications and prevention strategies of oblique lateral interbody fusion technique. *Orthop Surg*, 10(2): 98–106.

3. He W, He D, Sun Y, *et al.*, 2020, Standalone oblique lateral interbody fusion vs. combined with percutaneous pedicle screw in spondylolisthesis. *BMC Musculoskelet Disord*, 21(1): 1–9.

4. Choi YH, Kwon SW, Moon JH, *et al.*, 2017, Lateral lumbar interbody fusion and in situ screw fixation for rostral adjacent segment stenosis of the lumbar spine. *J Korean Neurosurg Soc*, 60(6): 755.

5. Xie T, Wang C, Yang Z, *et al.*, 2020, Minimally invasive oblique lateral lumbar interbody fusion combined with anterolateral screw fixation for lumbar degenerative disc disease. *World Neurosurg*, 135: e671–e678.

6. Hu Z, He D, Gao J, *et al.*, 2021, The influence of endplate morphology on cage subsidence in patients with stand-alone oblique lateral lumbar interbody fusion (OLIF). *Global Spine J,* 13(1): 97–103.

7. Siu TL, Rogers JM, Lin K, *et al.*, 2018, Custom-made titanium 3-dimensional printed interbody cages for treatment of osteoporotic fracture–related spinal deformity. *World Neurosurg*, 111: 1–5.

8. Huiskes R, Ruimerman R, Van Lenthe GH, *et al.*, 2000, Effects of mechanical forces on maintenance and adaptation of form in trabecular bone. *Nature*, 405(6787): 704–706.

9. Tartara F, Bongetta D, Pilloni G, *et al.* 2020, Custom-made trabecular titanium implants for the treatment of lumbar degenerative discopathy via ALIF/XLIF techniques: rationale for use and preliminary results. *Eur Spine J*, 29(2): 314–320.

10. Taniguchi N, Fujibayashi S, Takemoto M, *et al.*, 2016, Effect of pore size on bone ingrowth into porous titanium implants fabricated by additive manufacturing: An in vivo experiment. *Mater Sci Eng C*, 59: 690–701.

11. Li F, Li J, Xu G, *et al.*, 2015, Fabrication, pore structure and compressive behavior of anisotropic porous titanium for human trabecular bone implant applications. *J Mech Behav Biomed Mater*, 46: 104–114.

12. Chang B, Song W, Han T, *et al.*, 2016, Influence of pore size of porous titanium fabricated by vacuum diffusion bonding of titanium meshes on cell penetration and bone ingrowth. *Acta Biomater*, 33: 311–321.

13. Zhang Z, Fogel GR, Liao Z, *et al.*, 2018, Biomechanical analysis of lumbar interbody fusion cages with various lordotic angles: A finite element study. *Comput Methods Biomech Biomed Eng*, 21(3): 247–254.

14. Xiao Z, Wang L, Gong H, *et al.*, 2011, A non-linear finite element model of human L4-L5 lumbar spinal segment with three-dimensional solid element ligaments. *Theor App Mech Lett*, 1(6): 064001.

15. Guo HZ, Tang YC, Guo DQ, *et al.*, 2020, Stability evaluation of oblique lumbar interbody fusion constructs with various fixation options: A finite element analysis based on three-dimensional scanning models. *World Neurosurg*, 138: e530–e538.

16. Huang SF, Chang CM, Liao CY, *et al.,* 2022, Biomechanical evaluation of an osteoporotic anatomical 3D printing posterior lumbar interbody fusion cage with internal lattice design based on weighted topology optimization. *Int J Bioprint,* 9(3): 410–421.

17. Chazal J, Tanguy A, Bourges M, *et al.*, 1985, Biomechanical properties of spinal ligaments and a histological study of the supraspinal ligament in traction. *J Biomech*, 18(3): 167–176.

18. Zhong ZC, Wei SH, Wang JP, *et al.*, 2006, Finite element analysis of the lumbar spine with a new cage using a topology optimization method. *Med Eng Phys*, 28(1): 90–98.

19. Yamamoto ISAO, Panjabi MM, Crisco TREY, *et al.*, 1989, Three dimensional movements of the whole lumbar spine and lumbosacral joint. *Spine*, 14(11): 1256–1260.

20. Schmoelz W, Huber JF, Nydegger T, *et al.*, 2003, Dynamic stabilization of the lumbar spine and its effects on adjacent segments: an in vitro experiment. *Clin Spine Surg*, 16(4): 418–423.

21. Chen SH, Tai CL, Lin CY, *et al.*, 2008, Biomechanical comparison of a new stand-alone anterior lumbar interbody fusion cage with established fixation techniques – a three-dimensional finite element analysis. *BMC Musculoskelet Disord*, 9(1): 1–10.

22. Liao CY, Chien CL, Pu TW, *et al.*, 2022, Assessment of lumbar vertebrae morphology by computed tomography in older adults with osteoporosis. *Curr Med Imaging*, 18(11): 1195–1203.

23. Cobian D, Heiderscheit B, Daehn N, *et al.*, 2011, Comparison of daily motion of the cervical and lumbar spine to ASTM F2423-11 and ISO 18192-1.2011 standard testing. *J ASTM Int*, 9(1): 1–10.

24. Li CH, Wu CH, Lin CL, 2020, Design of a patient-specific mandible reconstruction implant with dental prosthesis for metal 3D printing using integrated weighted topology optimization and finite element analysis. *J Mech Behav Biomed Mater*, 105: 103700.

25. Taniguchi N, Fujibayashi S, Takemoto M, *et al.*, 2016, Effect of pore size on bone ingrowth into porous titanium implants fabricated by additive manufacturing: an in vivo experiment. *Mater Sci Eng C*, 59: 690–701.

26. Implants for surgery — Preclinical mechanical assessment of spinal implants and particular requirements —Part 2: Spinal intervertebral body fusion devices. ISO 23089–2:2021.

27. Yang J, Cai H, Lv J, *et al.*, 2014, In vivo study of a self-stabilizing artificial vertebral body fabricated by electron beam melting. *Spine*, 39(8): e486–e492.

28. Wu SH, Li Y, Zhang YQ, *et al.*, 2013, Porous titanium-6 aluminum-4 vanadium cage has better osseointegration and less micromotion than a poly-ether-ether-ketone cage in sheep vertebral fusion. *Artif Organs*, 37(12): e191–e201.

29. Chon CS, Ko CW, Kim HS, 2015, Development of anterior lumbar interbody fusion (ALIF) PEEK cage based on the Korean lumbar anatomical information. *Int J Biomed Biol Eng*, 9(2): 151–154.

30. Lim KM, Park TH, Lee SJ, *et al.*, 2019, Design and biomechanical verification of additive manufactured composite spinal cage composed of porous titanium cover and PEEK body. *Appl Sci*, 9(20): 4258.